Available online at www.sciencedirect.com
ScienceDirect
Trans. Nonferrous Met. Soc. China 35(2025) 2273−2287
Transactions of Nonferrous Metals Society of China
www.tnmsc.cn

Microstructural evolution and mechanical properties of network-structure Ti_2AlC/TiAl composites prepared by spark plasma sintering

Dong-dong ZHU[1], Jiang-fei YAN[1,2], Yu-peng WANG[3], Duo DONG[1,3], Xiao-hong WANG[3], Teng-fei MA[3], Zun-jie WEI[4]

1. School of Materials Science and Engineering, Taizhou University, Taizhou 318000, China;
2. School of Materials Science and Engineering, Anhui Polytechnic University, Wuhu 241000, China;
3. Key Laboratory of Air-driven Equipment Technology of Zhejiang Province, Quzhou University, Quzhou 324000, China;
4. School of Materials Science and Engineering, Harbin Institute of Technology, Harbin 150001, China

Received 7 November 2023; accepted 24 June 2024

Abstract: Ti_2AlC/TiAl composites with a network structure were successfully prepared with carbon nanotubes and Ti−45Al−8Nb pre-alloyed powder using spark plasma sintering. The effects of sintering temperature (1200−1350 °C) on the microstructural evolution and mechanical properties were systematically investigated. The microstructure of Ti_2AlC/TiAl composites exhibits duplex, near-lamellar, and fully lamellar structures, as the sintering temperature increases from 1200 to 1350 °C. The network structured Ti_2AlC phase can refine the microstructure and the phase becomes discontinuous at high sintering temperatures. Notably, composites sintered at 1300 °C exhibit excellent mechanical properties, with the highest compressive strength (1921 MPa) and fracture strain (26%) at room temperature. Moreover, the ultimate tensile strength and fracture strain reach 537 MPa and 3.1% at 900 °C, and 485 MPa and 3.3% at 950 °C, respectively. The enhancement of the mechanical properties is attributed primarily to the load bearing, particle pull-out, and inhibition of crack propagation induced by Ti_2AlC particles.

Key words: Ti_2AlC/TiAl composites; microstructure; spark plasma sinter; high-temperature tensile property; strengthening mechanism

1 Introduction

With the rapid development of the aerospace and automotive industries, it is a formidable challenge to develop a high-temperature, lightweight structural material with superior mechanical properties for high-performance and low-energy engines [1,2]. TiAl alloys are regarded as one of the most promising candidates for replacing traditional nickel-based superalloys at high temperatures due to their low density, high specific strength, excellent high-temperature oxidation resistance, and creep resistance [3−5]. Specifically, TiAl alloys have been successfully used in low-pressure turbine blades, turbocharger wheels, etc. For example, the 4822 (Ti−48Al−2Cr−2Nb) alloy has been employed in the low-pressure turbine blades of the GEnx™-2B engine [6]. Furthermore, TNM, 45XD, and 47WSi alloys have been successfully applied to industrial gas turbines and automotive engine parts [7−10]. However, poor ductility and insufficient strength severely restrict their application.

The use of composite technology is a novel strategy for improving the mechanical properties of TiAl alloys at various temperatures [11,12]. TiAl

Corresponding author: Duo DONG, E-mail: dongduohit@163.com;
Teng-fei MA, E-mail: matengfeihit@163.com
https://doi.org/10.1016/S1003-6326(25)66814-2

composites, especially ceramic particles-reinforced TiAl composites, have been widely studied because of their simple preparation process, low cost, and controllable properties. Recently, TiAl composites reinforced with various ceramic particles (such as Ti_2AlC, Ti_2AlN, TiC, Y_2O_3, TiB_2, and WC) [13−16] have been prepared, and they exhibit excellent mechanical properties. LI et al [17] prepared a TiB_2-reinforced γ-TiAl composite via hot isostatic pressing. The tensile strength and strain of the TiAl composite were enhanced by the TiB_2-reinforcing phases. GUO et al [18] demonstrated that the addition of Y_2O_3 could refine the grains and enhance the room-temperature tensile strength and ductility of TiAl alloys.

Notably, the Ti_2AlC phase, which has a unique layered structure and extraordinary dual metallic and ceramic properties, is considered an ideal reinforcing phase for preparing TiAl-based composites with excellent comprehensive properties. LIU et al [19] successfully fabricated Ti_2AlC/TiAl composites with a full lamellar structure by spark plasma sintering (SPS), and the micro−nano-Ti_2AlC particles were uniformly dispersed in the matrix. The ultimate compressive strength of the composite at 850 °C is comparable to that of other TiAl alloys at 800 °C. Recently, LIU et al [20] successfully designed a Ti_2AlC/TiAl composite with bioinspired micro−nano laminated architecture that exhibited excellent compression properties at room temperature. The properties of TiAl composites are strongly affected by the distribution of ceramic particles. Recent studies have shown that continuous network reinforcement can increase strength without causing severe plasticity damage [21−23]. However, the strengthening and toughening mechanisms of TiAl composites reinforced with three-dimensional network-structured Ti_2AlC particles are mainly assessed based on compression tests, while the high-temperature tensile properties and the corresponding strengthening mechanisms of TiAl composites have rarely been reported.

In this study, Ti_2AlC/TiAl composites with a three-dimensional network structure were fabricated by SPS at different temperatures. The effects of sintering temperature on the microstructural evolution and mechanical properties of Ti_2AlC/TiAl composites were systematically investigated. Furthermore, the strengthening and toughening mechanisms induced by the three-dimensional network structure of the Ti_2AlC reinforcement at various temperatures were discussed. This study is expected to provide theoretical guidance for the structural design and high-temperature strengthening mechanism of TiAl composites.

2 Experimental

In this study, TiAl prealloyed powder and carbon nanotubes (CNTs) were used as the raw materials. Ti−45Al−8Nb (at.%) prealloyed powder was supplied by Sino-Euro Materials Technologies of Xi'an Co., Ltd. (China), and was prepared via the plasma rotating electrode method with a particle size range of 45−150 μm. CNTs with lengths of 10−30 μm and diameters of 10−20 nm were purchased from Zhongke Times Nano Co. Ltd. (China). The 0.6 wt.% CNTs were mixed with TiAl prealloyed powder in a planetary ball mill. The mass ratio of stainless-steel balls to powder was 3:1, and ball milling was performed at a speed of 300 r/min for 6 h. After ball milling, the CNTs were uniformly adhered to the powder, which was mainly spherical. Subsequently, the powder mixed added to a graphite mold. Finally, vacuum sintering was carried out in a LABOX−650F SPS furnace. The sintering was performed at 1200, 1250, 1300, and 1350 °C, with a heating rate of 100 °C/min and a holding time of 5 min. The sintering pressure was kept constant at 40 MPa and the sintering chamber pressure was less than 10 Pa. The size of each sintered compact was d30 mm × 15 mm. According to the sintering temperature, the composites were designated as TA-1200, TA-1250, TA-1300, and TA-1350.

Compression and tensile specimens were cut from the sintered compacts using a wire electrical discharge machine and polished with silicon carbide sandpaper before the mechanical properties were tested. Compression tests were carried out on an MTS−370.10 universal test machine at room temperature with dimensions of d6 mm × 9 mm and a constant strain rate of $1\times10^{-3}\ s^{-1}$. The tensile specimens were dog-boned-shaped and the gauge size was 15 mm × 2 mm × 2 mm. Tensile tests were performed on an MTS−370.10 universal test machine at 900 and 950 °C, while the strain rate was $1\times10^{-4}\ s^{-1}$. After the tensile test, the samples were quenched immediately to observe the

microstructures. In addition, for accuracy, the tensile and compression tests were repeated three times for each condition.

Phase analysis of the sintered composites was performed on an X-ray diffractometer with Cu K_α radiation (XRD, Empyrean, Netherlands). The microstructure of the composites was characterized by optical microscopy (OM, IE500M−T/R) and scanning electron microscopy (SEM, Hitachi SU8010) coupled with energy dispersive spectroscopy (EDS). The samples for OM and SEM analysis were polished using SiC emery paper (180#, 400#, 800#, 1200# and 2000#), followed by etching with Kroll's reagent ($HF:HNO_3:H_2O$=1:3:6, vol.%). Transmission electron microscopy (TEM) analysis was conducted on a TECNAI G2 F30−TEM instrument operating at 200 kV. The electron backscatter diffraction (EBSD) test was performed on an Oxford system with scanning step of 0.5 μm. The samples for EBSD examination were prepared by vibration polishing. The lamellar colony size and lamellar spacing were estimated using Nano Measure software.

3 Results and discussion

3.1 Microstructure evolution

Figure 1 shows the XRD patterns of the TiAl composites sintered at different temperatures. The TiAl composites sintered at different temperatures consist of Ti_2AlC, γ, and α_2 phases, and impurity phases are also observed. The higher intensity of the diffraction peaks of the γ and Ti_2AlC phases can be detected in the TA-1200 composite. This is attributed to the sintering temperature located in the $\alpha+\gamma$ phase region, resulting in a large amount of

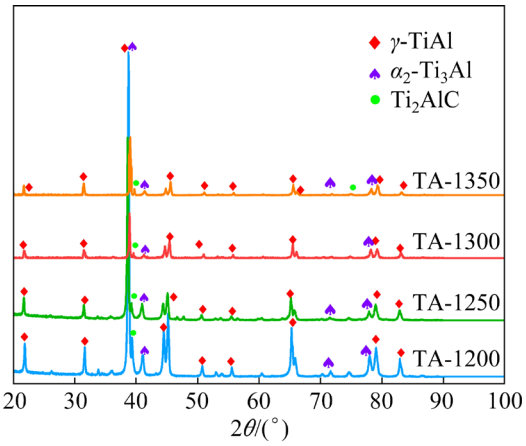

Fig. 1 XRD patterns of SPS sintered samples

γ-phase remaining after cooling. Furthermore, the solubility of C atoms in the γ phase is lower than that in the α_2 phase [24], which results in more significant Ti_2AlC precipitation. Upon further increasing the sintering temperature, the phase and diffraction peaks do not change significantly, which indicates that the reaction is complete during sintering at 1200 °C.

Figure 2 presents the metallographic microstructure of the as-sintered TiAl composites. The microstructure of the TiAl composites changes significantly with increasing sintering temperature. As illustrated in Fig. 2(a), the microstructure of the TA-1200 composite is composed of a duplex phase (DP), which indicates that the sintering temperature is located in the $\alpha+\gamma$ region. During cooling, the ordering transformation of $\alpha\rightarrow\alpha_2+\gamma$ occurs, while the γ phase is retained to form small equiaxed grains. When the temperature increases to 1250 °C, the composite has a near-lamellar (NL) microstructure consisting of ($\alpha_2+\gamma$) lamellar colonies and a small amount of equiaxed γ-phase, as shown in Fig. 2(b). The TA-1300 and TA-1350 composites are fully lamellar (FL) (Figs. 2(c, d)) because the sintering temperature is located in the α single-phase region when the temperature reaches 1300 °C. During the cooling process, the $\alpha\rightarrow\alpha+\gamma\rightarrow$ ($\alpha_2+\gamma$) transformation occurs, which results in an FL microstructure.

Figure 3 displays the SEM images of the TiAl composites sintered at different temperatures. Obviously, there are no defects or particle boundaries in the sintered samples, indicating that the samples are compact after sintering. As shown in Figs. 3(a−d), network-structured reinforcements can be observed in the composites. This can be attributed to the uniform dispersion of CNTs on the TiAl powder surface after ball milling, which form a network-structured carbide by the in-situ reaction with TiAl during sintering. It has been reported that this carbide exists as Ti_2AlC at high temperatures (>1000 °C) [25,26]. When the sintering temperature increases to 1300 °C, the network structure becomes discontinuous, and a small amount of micro−nano Ti_2AlC particles precipitate at the interfaces between the γ and α_2 lamellae, as illustrated in the magnified image in Fig. 3(c). This may be due to the low solubility of C in the TiAl matrix, which leads to the precipitation of Ti_2AlC particles.

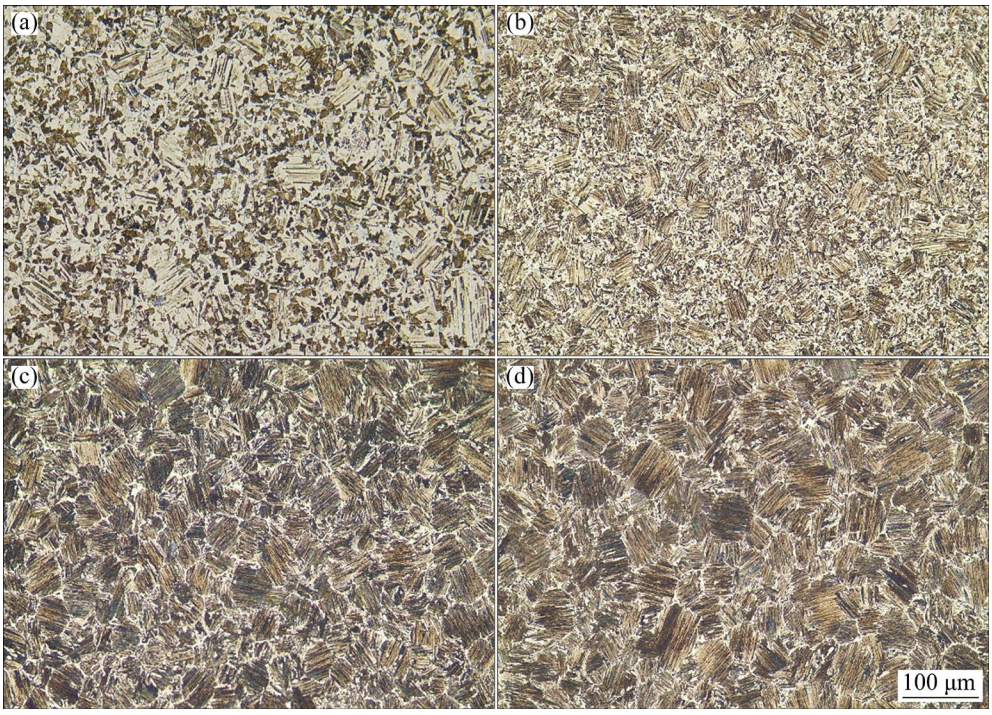

Fig. 2 Metallographic microstructures of TiAl composites prepared at different temperatures: (a) TA-1200; (b) TA-1250; (c) TA-1300; (d) TA-1350

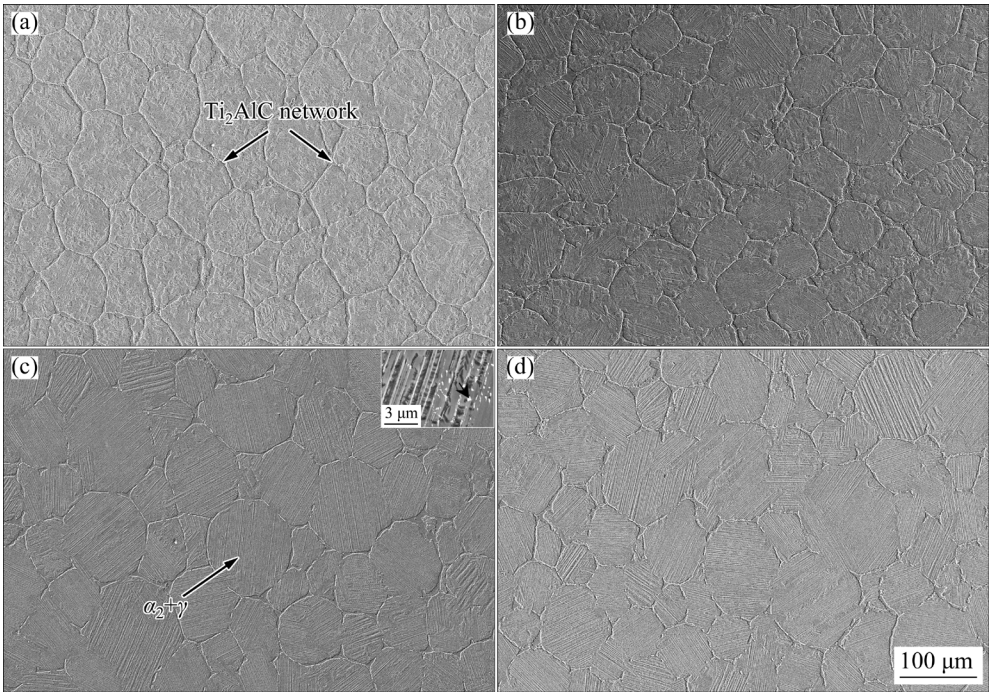

Fig. 3 SEM images of TiAl composites prepared at different temperatures: (a) TA-1200; (b) TA-1250; (c) TA-1300; (d) TA-1350

Figure 4 shows the average lamellar spacing and lamellar colony size of the TiAl composites. The average lamellar colony size increases from 44.93 to 106.55 μm as the sintering temperature increases from 1200 to 1350 °C. The size of the original α/α_2 grains has a great influence on lamellar colony size. At 1200 °C, γ grains nucleate and grow at the α phase interface, which inhibits the growth of the α phase, and results in a fine lamellar colony. When sintering at 1350 °C, the temperature

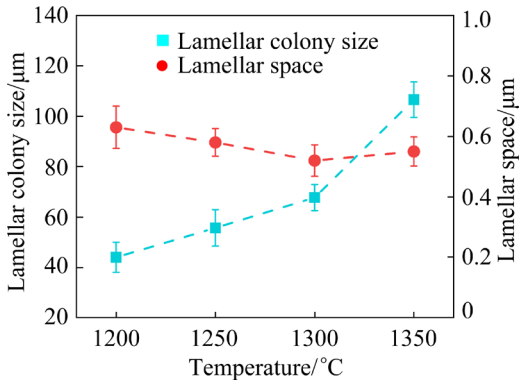

Fig. 4 Lamellar colony size and lamellar spacing of TiAl composites prepared at 1200−1350 °C

is completely located in the α single-phase region. The lamellar colony is susceptible to coarsening because the α phase grows without restriction. Furthermore, there is no significant change in the lamellar spacing (approximately 0.6 μm), because the lamellar spacing is mainly determined by the cooling rate [27]. In this work, all the sintered samples are cooled in circulating water to room temperature.

The phase composition of the TA-1300 composite was further characterized by SEM and EDS, as shown in Fig. 5. The results reveal that precipitates at the lamellar colony boundaries are enriched in Ti and C, while the contents of Al and Nb are relatively poor at the corresponding locations. In addition, the atomic ratio of precipitated phase is Ti:Al:C:Nb=43.15:26.73:26.18:3.94 (Fig. 5(f)). Combined with the XRD results in Fig. 1, the precipitates can be determined to be Ti_2AlC phases. These network Ti_2AlC phases nucleate and grow at the boundaries among different powders during sintering, which can significantly inhibit grain growth and refine the microstructure [28]. As a result, the strength and plasticity of the composites are enhanced.

Figure 6 shows the phase volume fraction and distribution obtained from the EBSD results of the TA-1300 composite. The phase distribution map (Fig. 6(a)) clearly indicates that the TA-1300 composite consists mainly of (α_2+γ) lamellar colonies and network-structured Ti_2AlC particles. In addition, α_2 is shown in red, γ is shown in green, and Ti_2AlC is shown in blue. The corresponding phase volume fractions are 1.45%, 89.1%, and 9.45%, respectively. The inverse pole figure of the composite (Fig. 6(b)) indicates that multiple crystal orientations can be observed within one lamellar colony. This is attributed to the γ lamellae with six orientation variants precipitating from disordered α phases during cooling. According to Fig. 6(c), the overlap position between the corresponding pole figures of α_2 and γ can be observed, indicating the existence of the same orientation relationship between α_2 and γ. As well known, the lamellar structure is formed by the ordered transformation of α phase. The γ phase nucleates in the α grain, and then expands and grows along the $(0001)_{\alpha_2}$ habit plane through a ledge mechanism, which eventually leads to the lamellar structure. The α_2 and γ lamellae within the same grain follow the Blackburn orientation relationship, i.e., $(0001)_{\alpha_2}//(111)_{\gamma}$, and $[11\bar{2}0]_{\alpha_2}//[1\,\bar{1}0]_{\gamma}$. The orientation relationship between the in situ synthesized Ti_2AlC particles and the γ-TiAl interface satisfies $(0001)_{Ti_2AlC}//(111)_{\gamma}$.

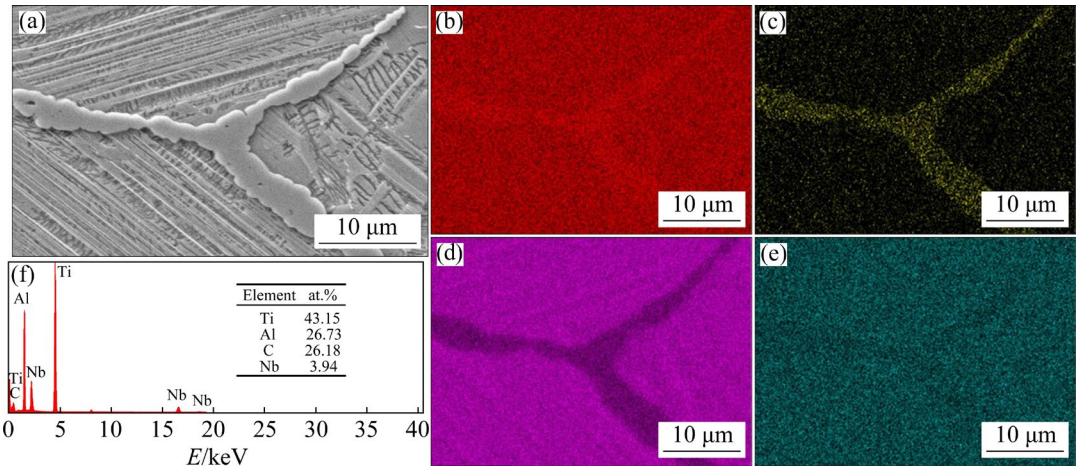

Fig. 5 SEM image of TA-1300 composite (a), corresponding EDS element distribution mappings of Ti (b), C (c), Al (d), Nb (e), and EDS point analysis result (f) in Fig. 5(a)

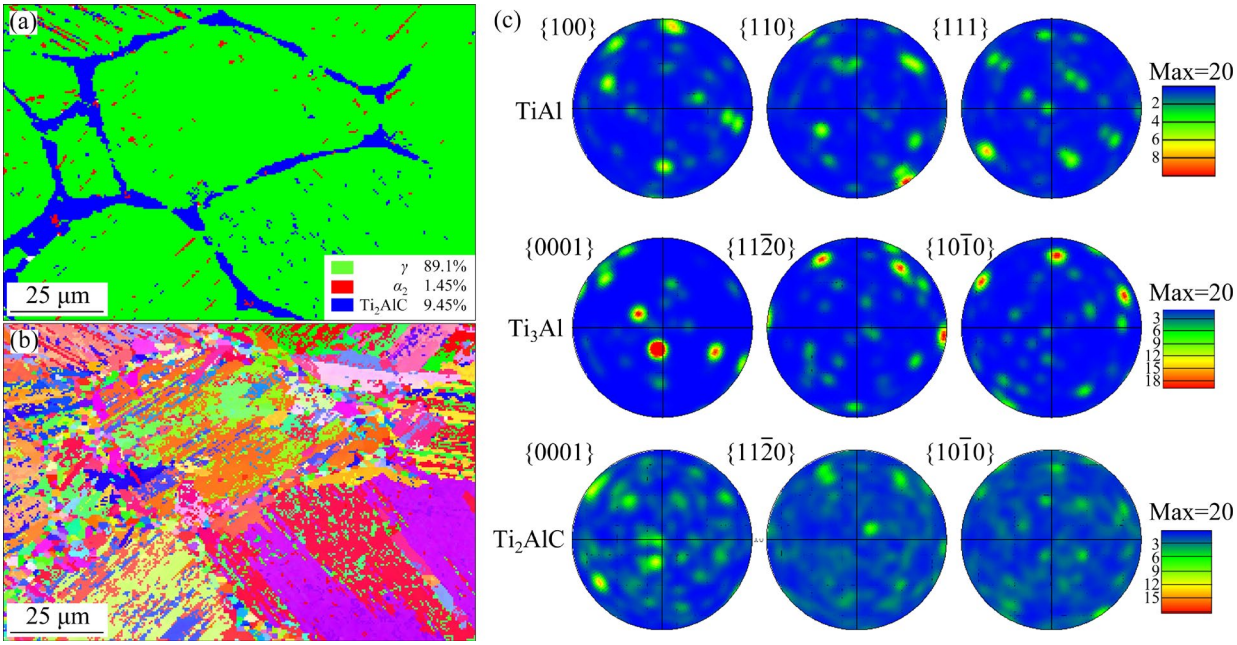

Fig. 6 EBSD analysis results of TA-1300 composites: (a) Phase distribution map; (b) Inverse pole figure; (c) Pole figure

The phase constituents and orientation relationships of the TA-1300 composite were investigated using TEM, as shown in Fig. 7. The parallel distributions of the γ and α_2 lamellae and the Ti_2AlC particle phase can be observed in Figs. 7(a, b). Figure 7(c) shows fast Fourier transform (FFT) and high-resolution TEM (HRTEM) images of the interfaces of α_2-Ti_3Al and γ-TiAl. The selective area electron diffraction (SAED) pattern displayed in Fig. 7(d) indicates that the γ and α_2 lamellae conform to the orientation relationship: $(0001)_{\alpha_2}//(111)_{\gamma}$, and $[11\bar{2}0]_{\alpha_2}//[1\bar{1}0]_{\gamma}$. The marked particle in Fig. 7(a) is further analyzed based on the SAED pattern, which is also identified as the Ti_2AlC phase with a space group of $P6_3/mmc$ (Fig. 7(e)). The STEM−EDS results in Figs. 7(f−i) show that the gray particle phase is rich in Ti and C and relatively lacking in Al, which further proves that the gray particle phase in Fig. 7(a) is Ti_2AlC.

Figure 8 shows schematic diagrams of the microstructural evolution of the TiAl composites during sintering. After mechanical ball milling, the CNTs are evenly distributed on the surface of the TiAl powder, and most of the powder particles are still spherical. During sintering, a high-temperature spark plasma can momentarily be generated between the powders under the action of a high electric-pulsed current. Then, the surface of the powder is activated, and the local temperature is elevated, which may result in localized melting of the powder. At the initial reaction stage, the CNTs participate in the diffusion reaction of Ti to form TiC. Then, Ti_2AlC is formed by the reaction of TiC and TiAl. In situ synthesized Ti_2AlC particles can obstruct grain boundary migration and refine grains [29]. According to Ti−Al−Nb ternary phase diagram [30], the $\alpha+\gamma$ phase region of the Ti−45Al−8Nb alloy is approximately 1200 °C, indicating that the matrix phase consists of α and γ phases at 1200 °C. During subsequent cooling, the α phase transforms to $(\alpha_2+\gamma)$ lamellae and retains the γ phase, eventually forming DP microstructure. At 1250 °C, the temperature is near the α phase transition temperature (T_α), and the microstructure consists mainly of the α phase and a few γ phases. After cooling, an NL microstructure consisting of a lamellar colony surrounded by γ is obtained. When the temperature further increases into α single-phase region (1300−1350 °C), the matrix is composed entirely of α phase. During subsequent cooling, phase transformation of $\alpha\rightarrow\alpha+\gamma\rightarrow\alpha_2+\gamma$ occurs, and an FL structure is formed.

3.2 Mechanical properties and fracture morphologies

In order to investigate the mechanical properties of the TiAl composites, compression tests were carried out on a universal test machine at

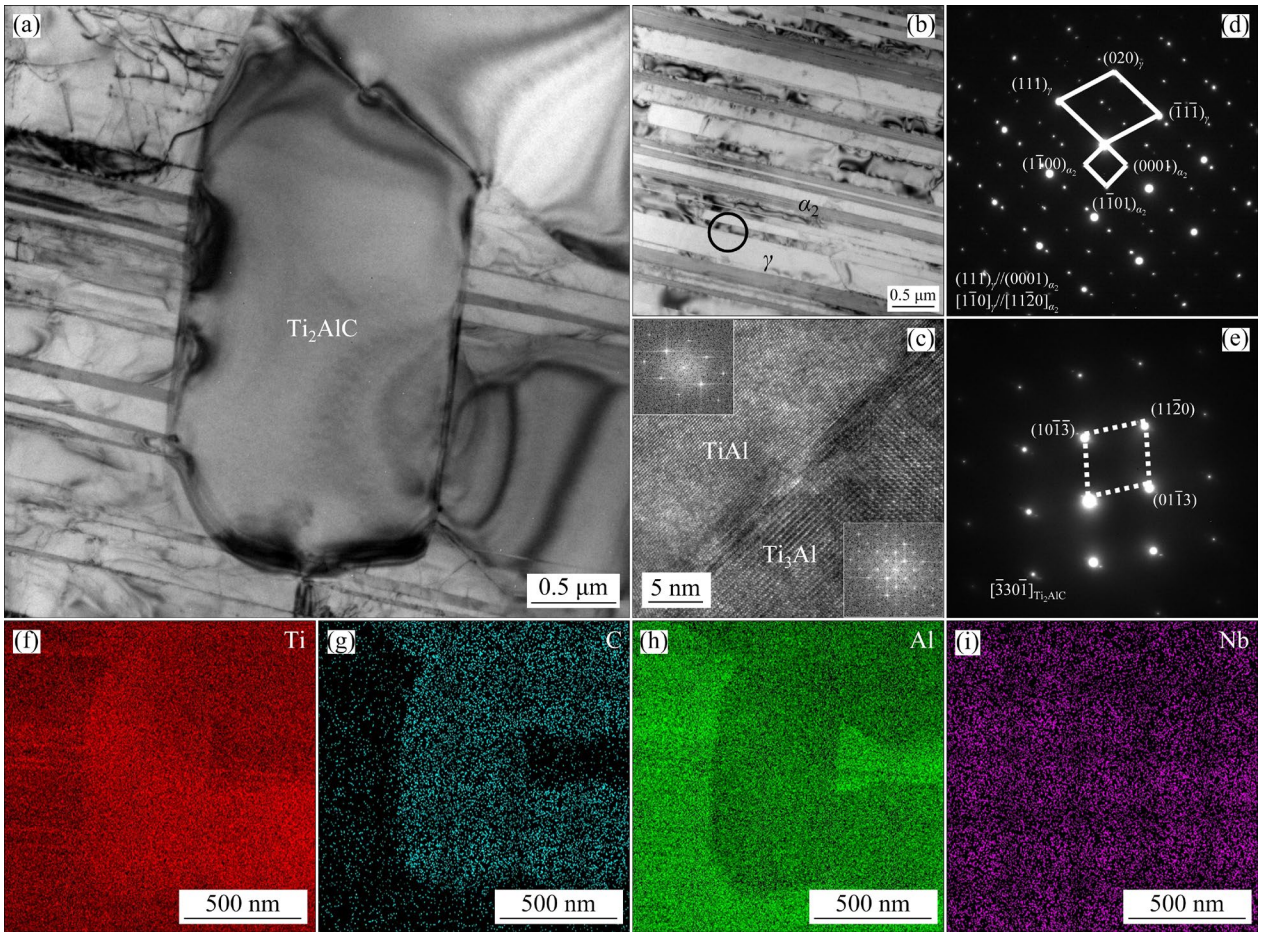

Fig. 7 Bright-field TEM images of TA-1300 composite (a, b), HRTEM image at α_2/γ interface (c), Orientation relationship of γ and α_2 (d), SAED pattern of Ti_2AlC (e), STEM−EDS maps (f−i) of (a)

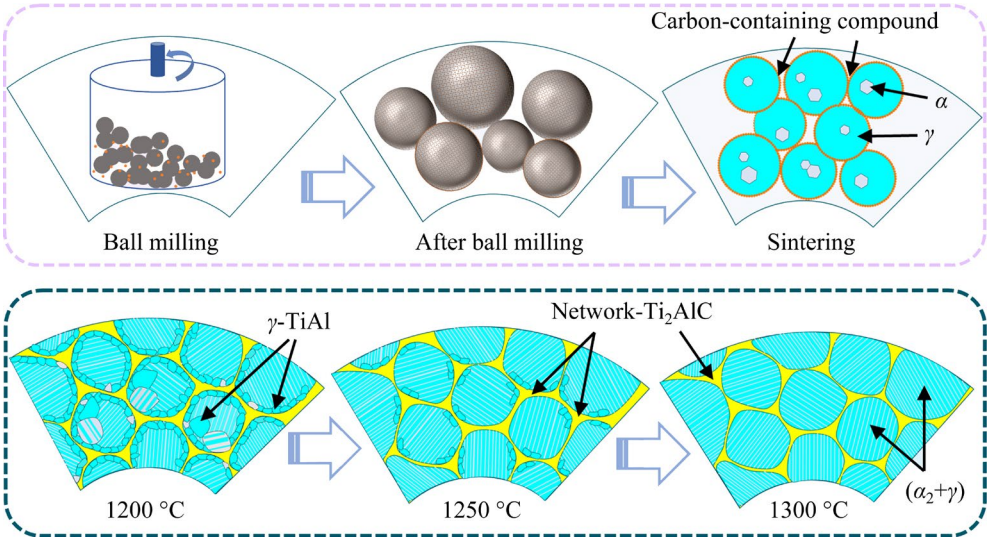

Fig. 8 Schematic illustrations of microstructural evolution of TiAl composites during SPS

room temperature. The engineering stress–strain curves and corresponding compressive properties are shown in Fig. 9. The composites exhibit significant plastic deformation before fracture, including three stages: (1) an elastic deformation stage at a strain of less than 8%, (2) a plastic deformation stage from 8% to the stage before fracture, and (3) a fracture stage. With increasing

sintering temperature, the compressive strength and fracture strain of the composites first increase and then decrease. The TA-1300 composite exhibits a maximum compressive strength and fracture strain of approximately 1921 MPa and 26%, respectively. The strength and fracture strain of the TA-1350 composite decrease to 1803 MPa and 22%, respectively. Compared to other composites, the TA-1300 composite exhibits best mechanical properties due to its homogeneous and fine fully lamellar microstructure.

Figure 10 shows the fracture morphologies of the TiAl composites after compression failure. The TiAl composites exhibit a typical brittle fracture mode, with mainly trans-lamellar and interlamellar fractures characteristics. The trans-lamellar fracture is formed due to the shear stress being perpendicular to the direction of the lamellae or forming a slight angle, and the fracture morphology shows the characteristics of a tearing ridge. The interlamellar fracture is attributed to the nucleation of microcracks at the α_2 and γ lamellar interfaces and propagation along the lamellae to form smooth planes. The fracture mode of the TA-1200 composite is intergranular fracture, and secondary cracks and a small amount of tear ridge features are observed in Fig. 10(a). The fracture pattern of the TA-1250 and TA-1300 composites is mainly

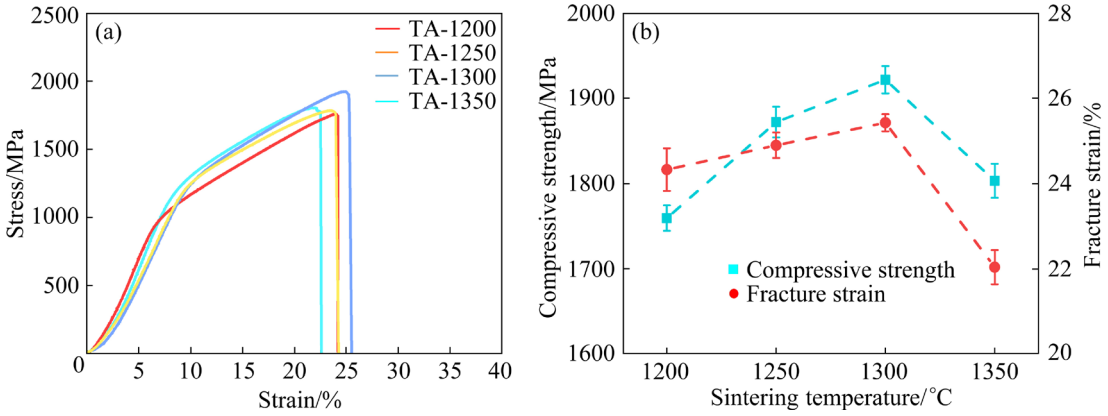

Fig. 9 Room temperature compressive curves of TiAl composites (a), and corresponding compressive strength and fracture strain (b)

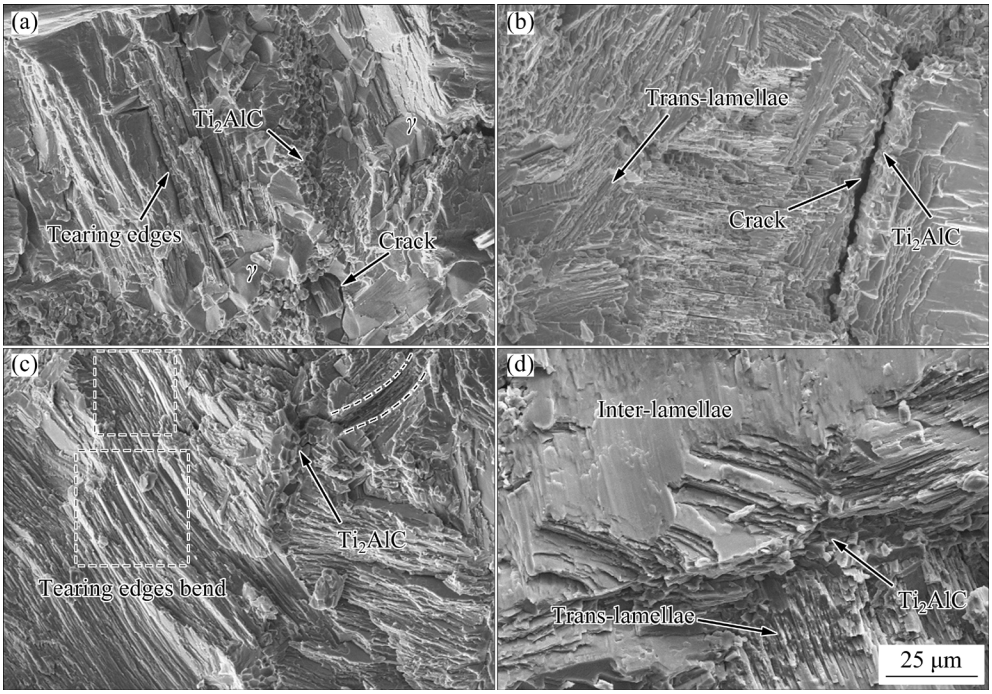

Fig. 10 Room-temperature compression fracture morphologies of TiAl composites: (a) TA-1200; (b) TA-1250; (c) TA-1300; (d) TA-1350

trans-lamellar, with cracks requiring a greater load to cut through the lamellar structure. The fracture morphology of the TA-1350 composite is shown in Fig. 10(d), which shows that interlamellar fracture is the primary fracture pattern. The microcracks nucleate at the α_2/γ interfaces and propagate along the interfaces. The fracture surface forms a great number of facets, which may result in the poor plasticity of TiAl alloys [31]. Notably, cracks or tear steps in the vicinity of Ti_2AlC are observed in all fracture morphologies after compression, indicating that Ti_2AlC plays a role in transferring loads and hindering crack propagation.

Tensile tests of the composites were conducted at 900 and 950 °C, and the corresponding engineering stress–strain curves are shown in Figs. 11(a, b). The tensile test curves reveal that the ultimate tensile strength of the composites first increases and then decreases with increasing sintering temperature. The TA-1200 composite exhibits the lowest ultimate tensile strength and the lowest fracture strain, of approximately 461 MPa and 2.5%, respectively. The TA-1300 composite with a fine full-lamellar microstructure has a maximum tensile strength of 537 MPa. However, as the temperature increases to 1350 °C, the ultimate tensile strength and fracture strain decrease to 496 MPa and 2.9%, respectively. The tensile test results at 950 °C are shown in Fig. 11(b). The engineering stress–strain curves before fracture of the composites all become flat, and the fracture strength decreases compared to that of the samples at 900 °C. Noteworthy, the TA-1300 composite still maintains a high ultimate fracture strength of 485 MPa at 950 °C. The fracture mechanisms are further discussed and analyzed in combination with the fracture morphologies.

Figure 11(c) shows a comparison of the high-temperature tensile properties at different temperatures between the network-structured Ti_2AlC/TiAl composites prepared in this work and other TiAl alloys (prepared by casting or powder metallurgy) [32−41]. SUN et al [32] studied the microstructure and properties of as-sintered and as-forged Ti−45Al−10Nb composites reinforced with Ti_2AlC particles. The tensile fracture strength of the composites was only 410 MPa at 900 °C (compared to a fracture strength of 537 MPa at 900 °C in this work). LAPIN et al [33] prepared in-situ carbide particle-reinforced TiAl composites

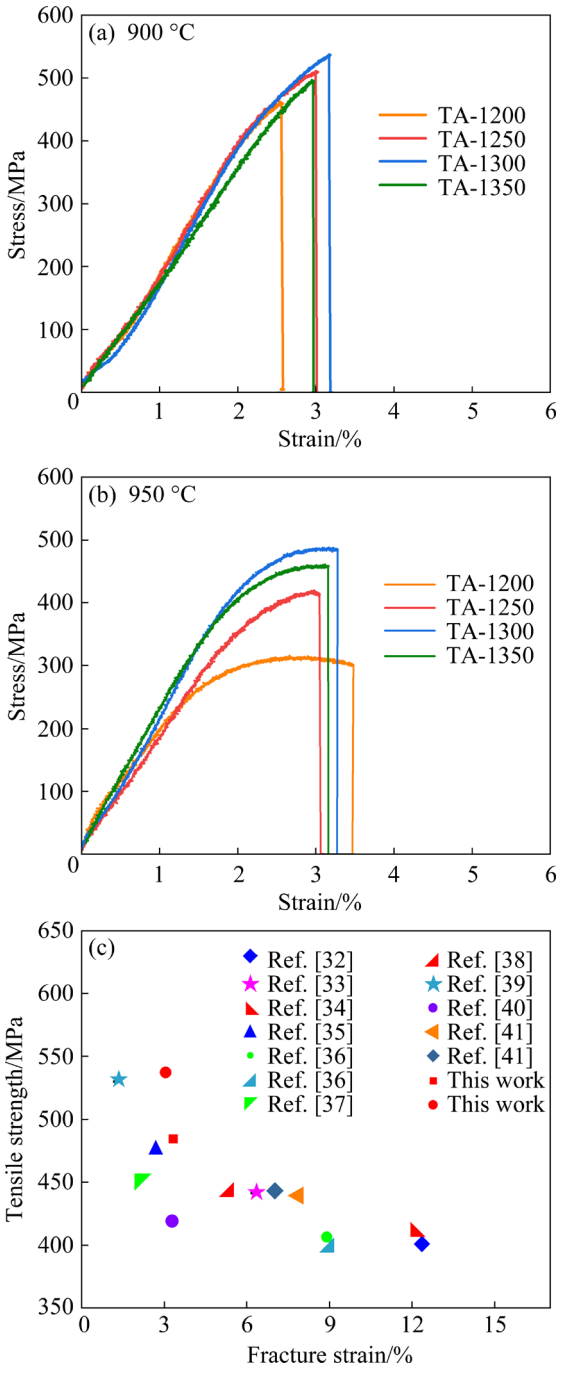

Fig. 11 High-temperature tensile engineering stress–strain curves of composites tested at 900 °C (a) and 950 °C (b), and comparison of tensile properties of composites with other alloys (c)

by vacuum induction melting and studied their high-temperature deformation behavior. The tensile fracture strength of the TiAl composites was close to 300 MPa at 950 °C (compared to a fracture strength of 485 MPa at 950 °C in this work). It appears that the strength of the composite prepared in this work is better than that of other TiAl alloys

prepared by different optimization methods and traditional casting methods. In summary, our research improves the high-temperature strength and service temperature of TiAl composites and significantly reduces the plastic loss.

The fracture morphologies of the TiAl composites after tensile tests at 900 and 950 °C are shown in Fig. 12. Distinct river patterns and stepped and rock candy morphologies can be observed in TA-1200 (Figs. 12(a, b)). This shows a mixed fracture mode of trans-lamellar fracture and intergranular fracture. For the TA-1250 composite, a stepped morphology and a few smooth cleavage planes can be observed on the fracture surface of the composite (Figs. 12(c, d)). The TA-1300 and TA-1350 composites exhibit the typical mixed modes of trans-lamellar fracture and interlamellar fracture (Figs. 12(e−h)). The fracture morphologies of the composites after tensile tests at 900 and 950 °C are very similar, indicating that the fracture

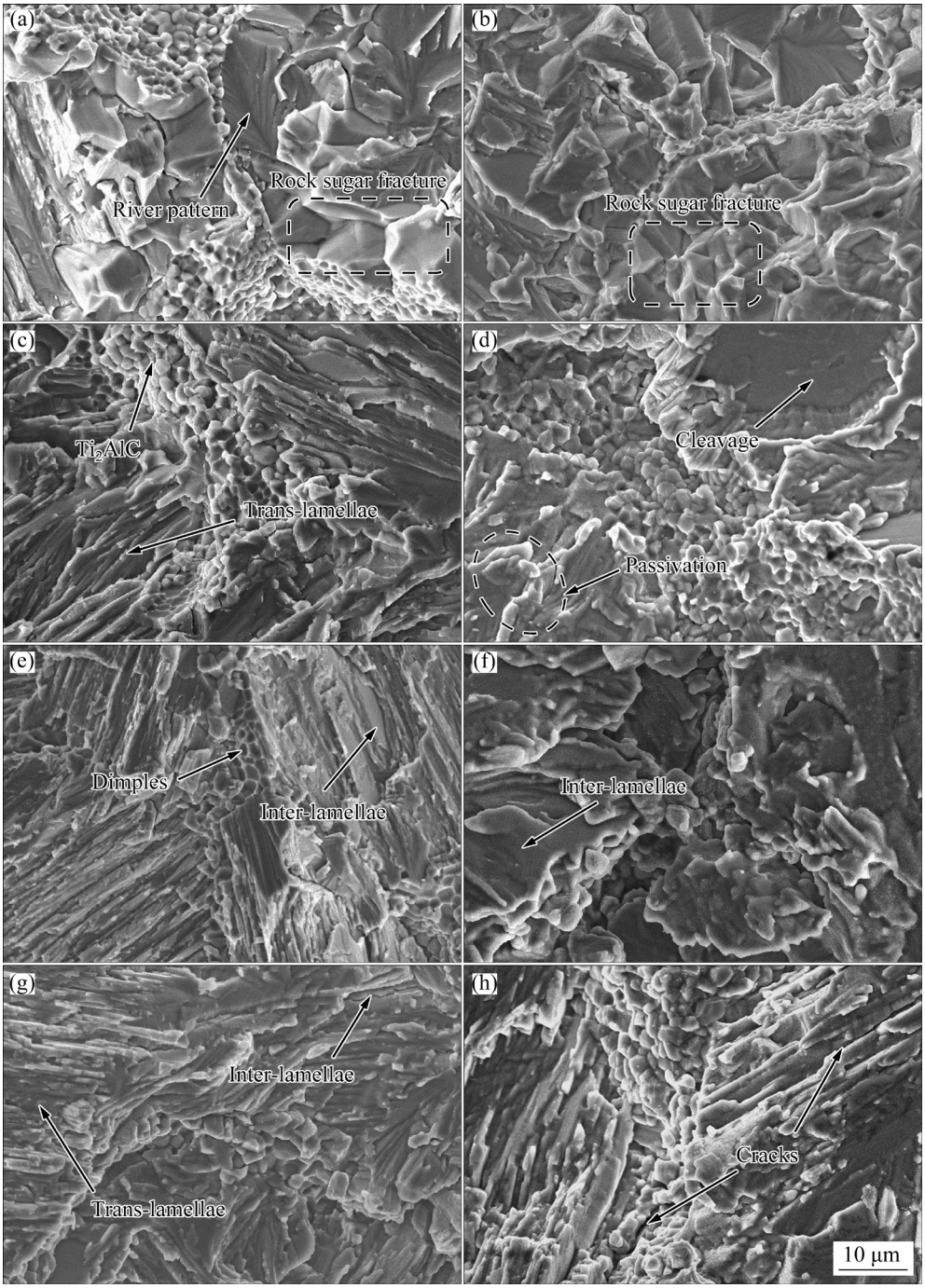

Fig. 12 Tensile fracture morphologies of TiAl composites tested at 900 °C (a, c, e, g) and 950 °C (b, d, f, h): (a, b) TA-1200; (c, d) TA-1250; (e, f) TA-1300; (g, h) TA-1350

mechanisms do not change at different test temperatures. In addition, dimples can be observed at the fracture surface, which can be attributed to the peeling of Ti_2AlC from the matrix. This is the main strengthening and toughening mechanism of TiAl composites.

Generally, the main plastic deformation mechanism of TiAl alloys is dislocation activity, such as dislocation multiplication, dislocation accumulation, and dislocation interaction in slip systems. It can be observed in Fig. 13 that the microcracks nucleate at the colony boundaries as well as at the α_2/γ lamellar interface and propagate along the Ti_2AlC/matrix interface with a partial tear in the Ti_2AlC phase. This indicates that Ti_2AlC can hinder dislocation slip during deformation and strengthen the grain boundaries, which can prevent cracks from passing directly through contiguous

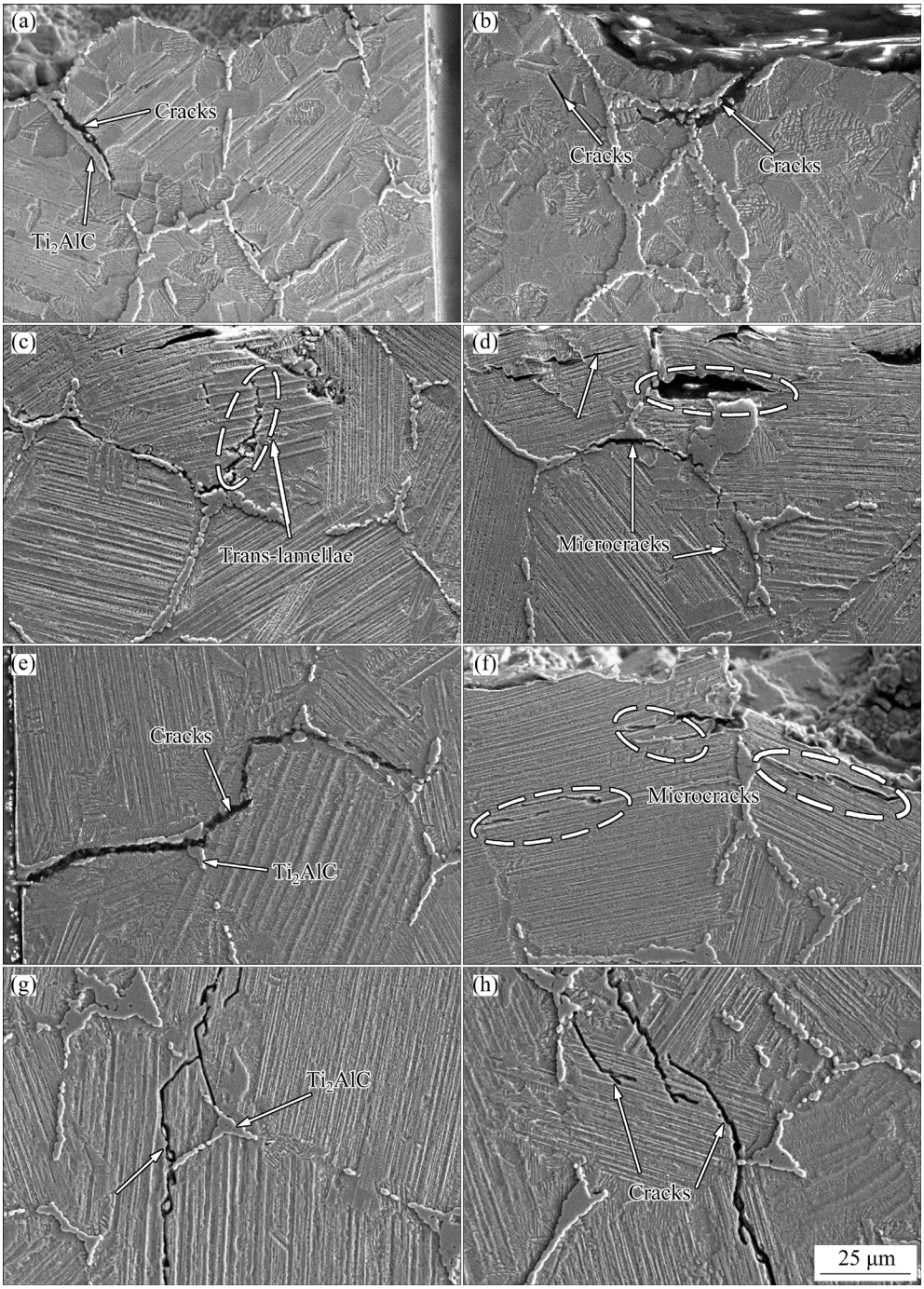

Fig. 13 SEM images of crack extension in composites tested at 900 °C (a, c, e, g) and 950 °C (b, d, f, h): (a, b) TA-1200; (c, d) TA-1250; (e, f) TA-1300; (g, h) TA-1350

grains and deflect the crack direction several times. During the fracture process, the energy required for crack propagation is consumed, thereby increasing the fracture strength of the composites. More cracks are observed on the side of the failed sample at 950 °C than at 900 °C (Figs. 13(b, d, f, h)). This is because thermal activation promotes dislocation movement and a high interfacial sliding drive force is produced, thereby facilitating crack initiation at 950 °C.

Figures 14(a, b) display the EBSD results near the fracture of the TA-1300 composite after tensile tests at 900 °C. A band contrast diagram is shown in Fig. 14(a), which reveals that the crack propagates and deflects along the edge of the Ti_2AlC grain. The (α_2+γ) lamellae near the cracks are bent, indicating

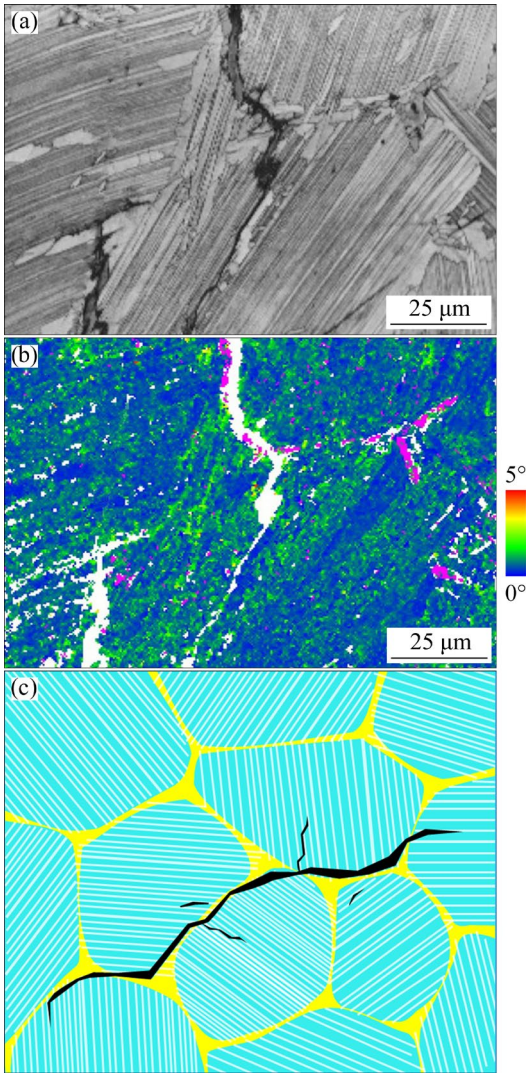

Fig. 14 Band contrast diagram (a), local misorientation in vicinity of crack fracture obtained by EBSD (b), and diagram of microscopic fracture mechanism of TiAl composites (c)

that the lamellar colony is subjected to a large deformation during the tensile test. As shown in Fig. 14(b), the crack expansion is hindered by the network-structured Ti_2AlC phase, resulting in severe deformation of the lamellae in the vicinity of the cracks and a high misorientation concentration at the corresponding locations. This indicates that the lamellar colonies are significantly deformed during the tensile deformation process, resulting in a remarkable stress concentration.

The fracture mechanism of Ti_2AlC/TiAl composites is summarized in Fig. 14(c). The microcracks caused by the stress concentration preferentially initiate at the tri-boundaries and α_2/γ lamellar interfaces, and then the cracks propagate along the interface of the Ti_2AlC/TiAl matrix and α_2/γ lamellae. During tensile tests, Ti_2AlC acts as a hard phase to bear more load. CHEN et al [15] measured the nanoindentation hardness of the Ti_2AlC phase to be 11.4 GPa. In addition, they found that Ti_2AlC acts as a barrier during deformation, which deflects the crack propagation direction and improves the strength and ductility. When cracks propagate to the discontinuous Ti_2AlC phase, they extend through the Ti_2AlC phase into the (α_2+γ) lamellar colonies in a zig-zag pattern. When the direction of crack extension is the same as that of the lamellae, the crack can easily penetrate into the entire lamellar colony. From the above analysis, it can be concluded that continuous network-structured Ti_2AlC phases can impede the glide of dislocation sources during testing, deflect the direction of crack propagation, and consume the energy required for crack extension, thus improving the high-temperature strength and ductility of TiAl alloys.

4 Conclusions

(1) A three-dimensional network of Ti_2AlC reinforcement can be synthesized in situ by adding CNTs to TiAl pre-alloyed powders. The Ti_2AlC phase is distributed in the matrix as a network and inhibits grain growth, which results in a fine microstructure.

(2) With increasing sintering temperature, the precipitation of the Ti_2AlC phase becomes discontinuous. In the temperature range of 1200−1300 °C, the composites are duplex, nearly lamellar, and fully lamellar. At 1350 °C, the

lamellar colonies become coarse.

(3) The network-structured Ti_2AlC/TiAl composites exhibit excellent mechanical properties. The compressive strength and fracture strain of the TA-1300 composite at room temperature are 1921 MPa and 26%, respectively; the ultimate tensile strength and fracture strain at 900 °C are 537 MPa and 3.1%, respectively.

(4) During compression and tensile tests, Ti_2AlC can act as a hard phase to bear more load, deflect the crack propagation direction and consume the energy for crack expansion, thereby increasing the strength and ductility of the TiAl alloy.

CRediT authorship contribution statement

Dong-dong ZHU: Methodology, Writing − Original draft, Validation; **Jiang-fei YAN:** Data curation, Writing − Review & editing; **Yu-peng WANG:** Validation, Methodology; **Duo DONG:** Methodology, Project administration; **Xiao-hong WANG:** Supervision; **Teng-fei MA:** Supervision; **Zun-jie WEI:** Conception.

Declaration of competing interest

The authors declare that they have no known competing financial interests or personal relationships that could have appeared to influence the work reported in this paper.

Acknowledgments

This work was financially supported by the National Natural Science Foundation of China (Nos. 52171120, 52271106, 52071188), and the Natural Science Foundation of Zhejiang Province, China (No. LZY23E050001).

References

[1] LIU Pei, XIE Jing-pei, WANG Ai-qin. A recent research progress in TiAl matrix composites: A review [J]. Journal of Materials Science, 2022, 57: 16147−16174.

[2] ZHU Dong-dong, LIU Li, DONG Duo, WANG Xiao-hong, LIU Yang, CHEN Zhuang, WEI Zun-jie. Microstructure and compression behavior of in-situ synthesized Ti_2AlC reinforced Ti−48Al−2Cr alloy with carbon nanotubes addition [J]. Journal of Alloys and Compounds, 2021, 862: 158646.

[3] LI Xiao-bing, XU Hao, XING Wei-wei, CHEN Bo, SHU Lei, ZHANG Meng-shu, LIU Kui. Microstructural evolution and mechanical properties of forged β-solidified γ-TiAl alloy by different heat treatments [J]. Transactions of Nonferrous Metals Society of China, 2022, 32: 2229−2242.

[4] ZHU Dong-dong, YAN Jiang-fei, JIN Yu-liang, DONG Duo, WANG Xiao-hong, MA Teng-fei. Pressure-induced excellent corrosion resistance of Ti−45Al−8Nb alloy [J]. Materials Letters, 2024, 355: 135446.

[5] PAN Yu, LU Xin, LIU Cheng-cheng, HUI Tai-long, ZHANG Ce, QU Xuan-hui. Sintering densification, microstructure and mechanical properties of Sn-doped high Nb-containing TiAl alloys fabricated by pressure-less sintering [J]. Intermetallics, 2020, 125: 106891.

[6] DUAN Bao-hua, YANG Yu-chen, HE Shi-yu, FENG Qi-sheng, MAO Lu, ZHANG Xue-xian, JIAO Li-na, LUA Xiong-gang, CHEN Guang-yao, LI Chong-he. History and development of γ-TiAl alloys and the effect of alloying elements on their phase transformations [J]. Journal of Alloys and Compounds, 2022, 909: 164811.

[7] ZHU Dong-dong, TANG Fu-hao, DONG Duo, WANG Xiao-hong, MA Teng-fei. Phase formation and nanohardness of Ti−48Al−2Cr−2Nb−1.5C alloy by melt spinning: The effect of cooling rates [J]. Vacuum, 2024, 222: 112985.

[8] HELMUT C, WILFRIED S. Light-weight intermetallic titanium aluminides–status of research and development [J]. Advanced Materials Research, 2011, 278: 551−556.

[9] WANG Yong-zhe, LIU Xin-wang, DONG Duo, ZHU Dong-dong, DING Hong-sheng, CHEN Rui-run, GUO Jing-jie, FU Heng-zhi. Temperature-dependent mechanical properties and fracture behavior of directionally solidified Ti47Al2Cr2Nb alloy [J]. Journal of Materials Research and Technology, 2023, 25: 570−580.

[10] GAO Qiang, ZHANG Lai-qi, QIAO Yi, LIN Jun-pin. Diffusion bonding behaviour of β–γ TiAl alloys containing high niobium with Ti interlayer by spark plasma sintering [J]. Transactions of Nonferrous Metals Society of China, 2022, 32: 3973−3984.

[11] WANG Guo-feng, SUI Xiao-chong, LIU Qing, LIU Yong-kang. Fabricating Ti_2AlNb sheet with high tensile strength and good ductility by hot packed rolling the spark plasma sintered pre-alloyed powder [J]. Materials Science and Engineering A, 2021, 801: 140392.

[12] IMAN T, EHSAN G. Production methods of CNT-reinforced Al matrix composites: A review [J]. Journal of Composites and Compounds, 2020, 2: 1−9.

[13] LUO Yao-feng, LU Rui-yu, WANG Yan, LIU Bin, YANG Hai-tang, LIU Yong. Interfacial reaction in Al_2O_3 fiber reinforced TiAl matrix composite [J]. Transactions of Nonferrous Metals Society of China, 2023, 33: 1589−1602.

[14] JIANG Min-jin, SUN Hong-liang, LIU Rui, JIANG Xiao-song, ZHANG Ya-li, SUN Da-ming. Fabrication and mechanical properties of Ti_2AlN/TiAl composite with continuous network structure [J]. Transactions of Nonferrous Metals Society of China, 2023, 33: 1437−1451.

[15] CHEN Rui-run, TAN Ying-mei, FANG Hong-yuan, LUO Liang-shun, DING Hong-sheng, SU Yan-Qinq, GUO Jing-jie, FU Heng-zhi. Macro/microstructure evolution and mechanical properties of $Ti_{33.3}Al$ alloys by adding WC particles [J]. Materials Science and Engineering A, 2018, 725: 171−180.

[16] JIA Yi, LIU Zhi-dong, LI Sha, YAO Hao-ming, REN Zhong-kai, WANG Tao, HAN Jian-chao, XIAO Shu-long, CHEN Yu-yong. Effect of cooling rate on solidification microstructure and mechanical properties of TiB_2-containing TiAl alloy [J]. Transactions of Nonferrous Metals Society of China, 2021, 31: 391−403.

[17] LI Wei, YANG Yi, LI Ming, LIU Jie, CAI Dao-sheng, WEI Qing-song, YAN Chun-ze, SHI Yu-sheng. Enhanced mechanical property with refined microstructure of a novel γ-TiAl/TiB_2 metal matrix composite (MMC) processed via hot isostatic press [J]. Materials & Design, 2018, 141: 57−66.

[18] GUO Ying-chao, LIANG Yong-feng, LIN Jun-pin, YANG Fei. Influence of nano-Y_2O_3 addition on microstructure and tensile properties of high-Al TiAl alloys [J]. Materials Science and Engineering A, 2021, 11: 1048.

[19] LIU Cheng-ze, WANG Yu-peng, HAN Wei-zhong, MA Teng-fei, MA Dong-feng, ZHANG Yu-sheng. Achieving superior high-temperature strength and oxidation resistance of TiAl nanocomposite through in situ semicoherent MAX phase precipitation [J]. ACS Applied Materials Interfaces, 2022, 14: 8394−8403.

[20] LIU Pei, HOU Bo, WANG Ai-qin, XIE Jing-pei, WANG Zhen-bo. Balancing the strength and ductility of Ti_2AlC/TiAl composite with a bioinspired micro−nano laminated architecture [J]. Materials & Design, 2022, 220: 110851.

[21] SONG Xiao-jie, CUI Hong-zhi, HAN Ye, DING Lei, SONG Qiang. $Ti_2Al(C,N)$ solid solution reinforcing TiAl based composites: Evolution of a core-shell structure, interfaces, and mechanical properties [J]. ACS Applied Materials Interfaces, 2018, 10: 16783−16792.

[22] ZHOU Hai-tao, SU Yong-jun, LIU Na, KONG Fan-tao, WANG Xiao-peng, ZHANG Xi, CHEN Yu-yong. Modification of microstructure and properties of Ti−47Al−2Cr−4Nb−0.3W alloys fabricated by SPS with trace multilayer graphene addition [J]. Materials Characterization, 2018, 138: 1−10.

[23] CHENG Jun, ZHU Sheng-yu, YU Yuan, YANG Jun, LIU Wei-min. Microstructure, mechanical and tribological properties of TiAl-based composites reinforced with high volume fraction of nearly network Ti_2AlC particulates [J]. Journal of Materials Science & Technology, 2018, 34: 670−678.

[24] FANG Hong-ze, WANG Shu, CHEN Rui-run, XU Qin, YAN Yong-da, SU Yan-qing, GUO Jing-jie. The effects of the formation of a multi-scale reinforcing phase on the microstructure evolution and mechanical properties of a Ti_2AlC/TiAl alloy [J]. Nanoscale, 2021, 13: 12565.

[25] LIU Pei, HOU Bo, WANG Ai-qin, XIE Jing-pei, WANG Zhen-bo, YE Feng., Superior strength-plasticity synergy in a heterogeneous lamellar Ti_2AlC/TiAl composite with unique interfacial microstructure [J]. Journal of Materials Science & Technology, 2023, 159: 21−32.

[26] WANG Zhen-bo, LIU Pei, HOU Bo, YE Feng, WANG Ai-qin, XIE Jing-pei. Investigation on the in-situ reaction mechanism of Ti_2AlC/TiAl composite prepared by spark plasma sintering [J]. Materials Characterization, 2022, 194: 112417.

[27] CAO Bei, YANG Jie-ren, WANG Xu-yang, WU Yu-lun, HU Rui. Microstructure evolution and mechanical properties of a Ti−45Al−8.5Nb−(W,B,Y) alloy obtained by controlled cooling from a single β region [J]. Journal of Alloys and Compounds, 2017, 740: 1140−1148.

[28] ZHU Dong-dong, YAN Jiang-fei, WANG Yu-peng, JIN Yu-liang, DONG Duo, WANG Xiao-hong, MA Teng-fei, ZHU Liu. Enhancing the mechanical and tribological properties of TiAl alloy by network structured Ti_2AlC [J]. Journal of Materials Science, 2024, 59: 5399−5413.

[29] HOU Bo, LIU Pei, WANG Ai-qin, XIE Jing-pei. Fabrication, microstructure and compressive properties of Ti_2AlC/TiAl composite with a bioinspired laminated structure [J]. Vacuum, 2022, 201: 111124.

[30] LI Ming-ao, LI Juan, ZHOU Tao, HU Li, SHI Lai-xin, CHEN Yu-yong, XU Li-juan, XIAO Shu-long. Microstructure evolution, deformation behavior and manufacture design of TiAl matrix composites reinforced with in-situ borides precipitation [J]. Transactions of Nonferrous Metals Society of China, 2023, 33: 107−127.

[31] XU Xue-song, DING Hong-sheng, HUANG Hai-tao, LIANG He, CHEN Rui-run, GUO Jing-jie, FU Heng-zhi. Microstructure and elevated temperature tensile property of Ti−46Al−7Nb−(W,Cr,B) alloy compared with binary and ternary TiAl alloy [J]. Materials Science and Engineering A, 2021, 807: 140902.

[32] SUN Hong-fei, LI Xue-wen, ZHANG Peng, FANG Wen-bin. The microstructure and tensile properties of the Ti_2AlC reinforced TiAl composites fabricated by powder metallurgy [J]. Materials Science and Engineering A, 2014, 611: 257−262.

[33] LAPIN J, PELACHOVÁ T, BAJANA O. High temperature deformation behavior and microstructure of cast in-situ TiAl matrix composite reinforced with carbide particles [J]. Journal of Alloys and Compounds, 2019, 797: 754−765.

[34] XU Xue-song, DING Hong-sheng, HUANG Hai-tao, LIANG He, CHEN Rui-run, GUO Jing-jie, FU Heng-zhi. Effect of V on the microstructure and brittle-to-ductile transition of directionally solidified high-Nb TiAl alloy [J]. Intermetallics, 2022, 142: 107455.

[35] CHENG Liang, ZHANG Shuai-jin, YANG Guang, KOU Hong-chao, BOUZY E. Tailoring microstructure and mechanical performance of a β-solidifying TiAl alloy via martensitic transformation [J]. Materials Characterization, 2021, 173: 110970.

[36] FANG Hong-ze, CHEN Rui-run, LIU Yang-li, TAN Ying-mei, SU Yan-qing, DING Hong-sheng, GUO Jing-jie. Effects of niobium on phase composition and improving mechanical properties in TiAl alloy reinforced by Ti_2AlC [J]. Intermetallics, 2019, 115: 106630.

[37] PARK Ji-sung, YANG Guang, KIM Seong-woong. A high tensile strength above 900 °C in β-solidified TiAl alloy through alloy design and microstructure optimization [J]. Journal of Alloys and Compounds, 2023, 947: 169676.

[38] LIU Yang-li, ZHENG Wei-wei, FANG Hong-ze, YANG Yao-hua, CHEN Rui-run. Effect of cyclic DHT on microstructural evolution and mechanical properties of Ti−44Al−6Nb−1Cr−2V alloy [J]. Journal of Alloys and Compounds, 2023, 936: 168173.

[39] FANG Hong-ze, YANG Xiao-kang, ZHOU Ling-yan, CHEN Rui-run, ZHANG Yong, YAN Yong-da, SU Yan-qing. Exploration of homologous substitution element on phase ratio and high temperature properties in high Nb-containing TiAl alloy [J]. Journal of Alloys and Compounds, 2022, 918: 165782.

[40] WANG Hai-ling, WANG Qiang, DING Hong-sheng, CHEN Rui-run, ZENG Liang-cai. High-temperature tensile

behaviors and microstructural evolutions of a directionally solidified Ti−45Al−5Nb−2Mn alloy [J]. Materials Science and Engineering A, 2021, 825: 141904.
[41] LI Min-gao, XIAO Shu-long, CHENG Yu-yong, XU Li-juan, TIAN Jing. The effect of boron addition on the high-temperature properties and microstructure evolution of high Nb containing TiAl alloys [J]. Materials Science and Engineering A, 2018, 733: 190−198.

放电等离子烧结制备网络结构 Ti_2AlC/TiAl 复合材料的显微组织演变及力学性能

朱冬冬[1]，晏江飞[1,2]，王玉鹏[3]，董 多[1,3]，王晓红[3]，马腾飞[3]，魏尊杰[4]

1. 台州学院 材料科学与工程学院，台州 318000；
2. 安徽工程大学 材料科学与工程学院，芜湖 241000；
3. 衢州学院 浙江省空气驱动装备技术重点实验室，衢州 324000；
4. 哈尔滨工业大学 材料科学与工程学院，哈尔滨 150001

摘 要：利用碳纳米管和 Ti−45Al−8Nb 预合金粉末为原料，通过放电等离子烧结成功制备了具有网络结构的 Ti_2AlC/TiAl 复合材料。系统研究了烧结温度(1200～1350 ℃)对显微组织演变和力学性能的影响。结果表明，随着烧结温度从 1200 ℃升至 1350 ℃，复合材料显微组织呈现双态、近片层和全片层结构。网状结构的 Ti_2AlC 相能够细化组织，且随着温度的升高而变得不连续。在 1300 ℃下烧结的复合材料表现出最高的抗压强度和断裂应变，分别为 1921 MPa 和 26%。此外，复合材料在 900 ℃时的极限拉伸强度和断裂应变为 537 MPa 和 3.1%，在 950 ℃时仍然高达 485 MPa 和 3.3%。Ti_2AlC 承载载荷、颗粒拔出和抑制裂纹扩展是提高复合材料力学性能的主要原因。

关键词：Ti_2AlC/TiAl 复合材料；显微组织；放电等离子烧结；高温拉伸性能；强化机理

(Edited by Bing YANG)